aerospace

MDPI

Article

The Development of a 3D-Printed Compliant System for the Orientation of Payloads on Small Satellites: Material Characterization and Finite Element Analysis of 3D-Printed Polyetherketoneketone (PEKK)

Morgane Domerg [1,*], Benjamin Ostré [1], Yoann Joliff [1], Yves-Henri Grunevald [2,3] and Antoine Dubois Garcia [4]

1 MAPIEM, Université de Toulon, 83130 Toulon, France; benjamin.ostre@univ-tln.fr (B.O.); yoann.joliff@univ-tln.fr (Y.J.)
2 Laboratoire de Mécanique et d'Acoustique, AMU-CNRS-Centrale Méditerranée, UMR 7031, 4 Impasse Nikola Tesla, 13453 Marseille, France; yves-henri.grunevald@ces-works.com
3 CES WORKS, 131 Traverse Penne aux Camoins, BT 4 ID Dom Actiparc 1, 13821 La Penne-sur-Huveaune, France
4 SEMATEC METROLOGIE, HEXAGON, 158 Chemin du Vercors, 38260 La Frette, France; antoine.dubois@hexagon.com
* Correspondence: morgane.domerg@univ-tln.fr

Abstract: This article focuses on the development of a 3D-printed 2-degree-of-freedom (DOF) joint for the payloads' orientation on small satellites. This system is a compliant mechanism, meaning that this monolithic system composed of cross-axis flexural pivots (CAFPs) produces complex movements through the elastic deformation of its structure. Using fused filament fabrication (FFF), a demonstrator made of Polyetherketoneketone (PEKK) is printed to determine its potential compatibility with space conditions. Focusing on a segment of the joint, the CAFP, this study aims for an enhancement of its mechanical behavior through the study of its printing direction and the creation of an accurate finite element model of this compliant mechanism. First, material characterization of 3D-printed PEKK is achieved through differential scanning calorimetry tests of the filament and flexural and tensile tests of specimens printed in different printing directions. Then, these data are used to perform a finite element analysis of different CAFP designs and compare their mechanical response of their 3D-printed twin using digital image correlation software. Finally, the CAFP structures were observed by X-ray tomography. The results show that printing direction greatly influences both flexural and tensile strength. Voids induced by the FFF process could impact the mechanical behavior of 3D-printed parts as the simple CAFP design has a better test/model correlation than complex ones. This could influence its resistance to space environment.

Keywords: fused deposition modeling; aerospace engineering; compliant mechanisms; mechanical properties; finite element analysis

check for updates

Citation: Domerg, M.; Ostré, B.; Joliff, Y.; Grunevald, Y.-H.; Garcia, A.D. The Development of a 3D-Printed Compliant System for the Orientation of Payloads on Small Satellites: Material Characterization and Finite Element Analysis of 3D-Printed Polyetherketoneketone (PEKK). *Aerospace* **2024**, *11*, 294. https://doi.org/10.3390/aerospace11040294

Academic Editor: Paolo Marzioli

Received: 27 February 2024
Revised: 20 March 2024
Accepted: 8 April 2024
Published: 10 April 2024

1. Introduction

Compliant mechanisms are monolithic systems that produce complex movements through the elastic deformation of their structure. They have many applications, but they are mostly used in the medical [1], space [2], and precision domains [3,4]. Compliant mechanisms do not have backlash or wear, which leads to precise motions and absence of lubrication. These qualities are particularly relevant for space applications. This study forms part of the development of a 2-DOF compliant joint. In Figure 1, the prototype of the studied mechanism is presented. With a large rotation range of ±45°, this joint could be used to orient payloads on small satellites. It is composed of cross-axis flexural pivots (CAFPs), a well-documented compliant joint [5–7].

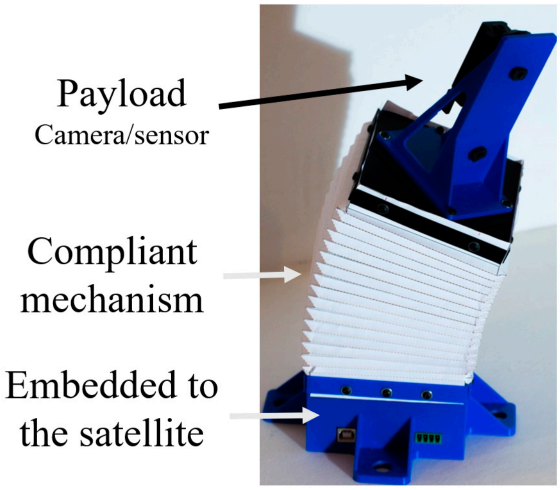

Figure 1. Three-dimensional-printed prototype of the compliant system.

As small satellites aim at improving space accessibility, this joint is polymeric and 3D printed using FFF. This process is usually used for single-use items and prototypes in a variety of domains. It is well established in the literature that, with FFF, mechanical properties are linked to printing parameters as they impact the internal structure, the inter and intra layers bonds, and the crystallization of the printed parts [8–10]. Among them, an influential parameter is printing direction. In [11], various printing directions are studied and show its heavy impact on stiffness, resilience, and maximum stress.

One concern about the spatialization of 3D-printed parts is the porosity induced by the FFF process that could impact their vacuum resistance. Indeed, various studies have attested to the presence of voids inside 3D-printed specimens [12,13]. They are mostly created between layers, and their shape and size are influenced by printing parameters.

Few are the polymers capable of withstanding space environment, but PEEK is a good candidate. The resistance of injecting PEEK to a vacuum environment has been attested [14]. Three-dimensional-printed conductive PEEK parts [15] and a PEEK nanosat structure [16] were developed using FFF and proved 3D-printed PEEK's low outgassing despite the porosity induced by the process.

Another potential candidate is PEKK. It is also a recent high-temperature polymer mostly used as matrix in fiber reinforced composites [17] for aerospace applications [18]. Biocompatible, it is also used for the creation of protheses [19,20]. It is this field that most literature about 3D-printed PEKK can be found, and only a few studies investigate the impact of printing parameters on tensile and flexural properties. The mechanical behavior of this material will be investigated in this study.

To our knowledge, when it comes to 3D-printed polymers for space applications, there are no compliant mechanisms that were studied for space applications.

This study is focused on a section of the 2-DOF compliant system, the CAFP, from its printing optimization to its finite element analysis. The material characterization of 3D-printed PEKK is carried out. First, DSC tests of the filament are carried out to gain a better understanding of the thermal properties of this material. Then, the mechanical properties resulting from different printing directions are studied through flexural and tensile tests. These data are used to create a finite element analysis of different CAFP designs. The mechanical response to their 3D-printed twin is compared using digital image correlation software. The pivots structures were observed by X-ray tomography.

2. Materials and Methods

2.1. Material

The filament used is PEKK-A, supplied by KIMYA (Nantes, France). According to the supplier, the filament used for this study has the properties described in Table 1.

Table 1. PEKK-A filament properties.

Diameter [mm]	1.75
Density [g/cm^3]	1.291
Tg [°C]	159
Tm [°C]	308

2.2. Process

2.2.1. Mechanical Characterization

In this study, the mechanical characterization of the 3D-printed filament consists of performing tensile tests, flexural tests, and density measurements. These data are essential for the optimization of printing parameters and for the development of the finite element analysis.

Figure 2 presents the two studied printing directions: "on edge" and "flat". For each direction, tensile and flexural tests are performed according to the tests standards ISO 527 [21] and ISO 178 [22], respectively. For each test and direction, 5 specimens are printed. The dimensions of these specimens and those used for density measurements are presented in Figure 3. For these last specimens, they were printed in batches of 10 for each printing direction.

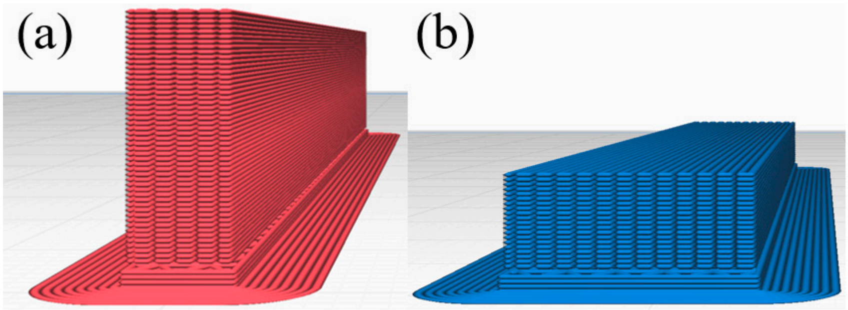

Figure 2. Printing orientation of flexural specimens: "on edge" (**a**) and "flat" (**b**).

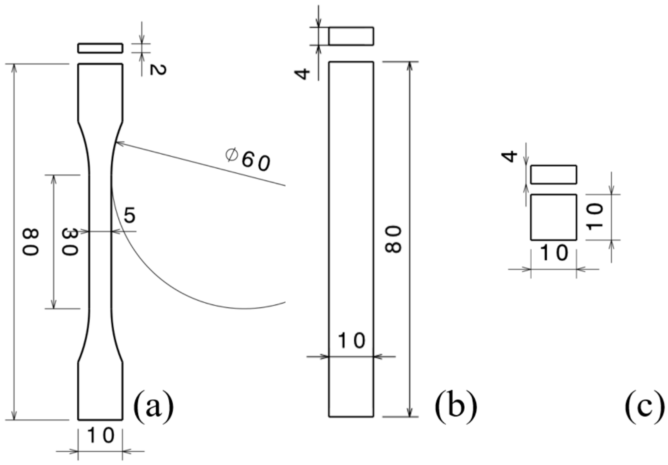

Figure 3. Dimensions of tensile specimens (ISO 527 test standard) (**a**), flexural specimens (ISO 178 test standard), (**b**) and the specimens used for density measurements (**c**).

2.2.2. Cross-Axis Flexural Pivots

In Figure 4, two different designs of CAFPs are tested. CAFP1, the first design, is well known among the compliant mechanisms community [5]. It is composed of 2 rectangular blades, whereas CAFP2, the second design, has a more complex design to improve compactness. Indeed, compared to the standard design, the thickness of CAFP2 is reduced by 56% and the weight is reduced by 44%. The blades have variable thicknesses and widths throughout their lengths.

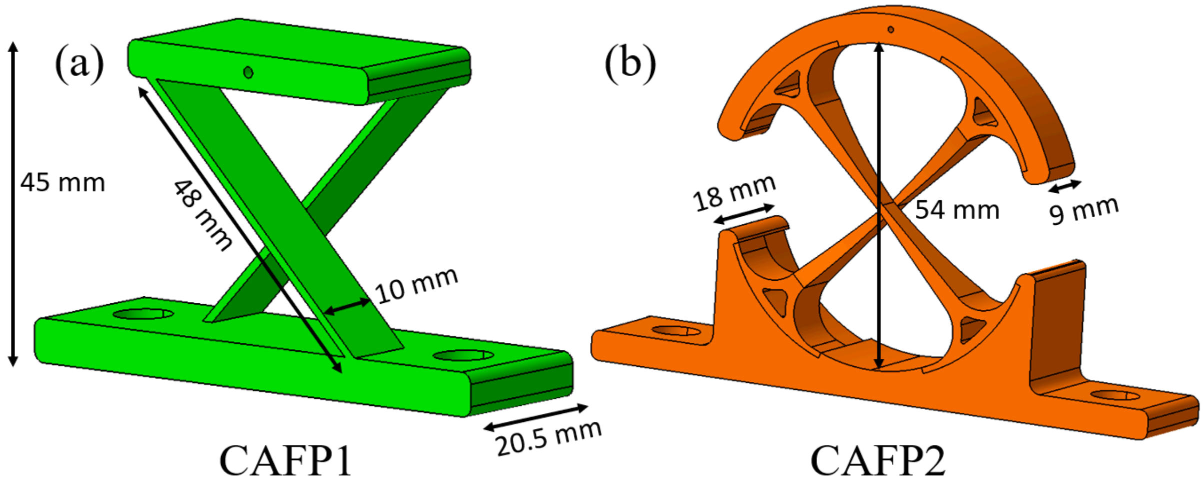

Figure 4. Design and dimensions of CAFP 1 (**a**) and CAFP 2 (**b**).

2.2.3. From CAD to Printing

All parts included in this study were designed on CATIA V5 and then transferred in STL format to the slicing software Cura 5.2.1 to define their printing parameters. The specimens and CAFP were printed using a Volumic Ultra SC2 printer. A ULTEM1000 adhesive was used to help the extruded filament stick to the print bed. Supports were printed between the parts and the bed to make their removal easier.

The common printing parameters of the specimens used for material characterization and the CAFPs are summarized in Table 2. However, their structures differ, so their resulting parameters are presented Figure 5 and Table 3.

Table 2. General printing parameters.

Layer thickness [mm]	0.2	Support height [mm]	0.8
Printing temperature [°C]	345	Support infill density [%]	70
Bed temperature [°C]	145	Support Z distance [mm]	0.1
Printing speed [mm/s]	25	Support type	triangular
Layer width [mm]	0.4	Support horizontal expansion [mm]	0.5

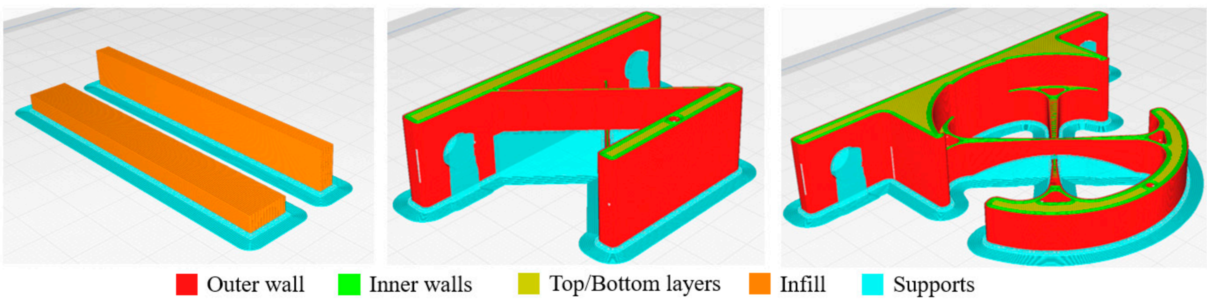

Figure 5. Flexural specimens and cross-axis flexural pivots on the printing bed.

Table 3. Structural printing parameters for the mechanical characterization and the pivots.

	Flexural, Tensile, and Density Specimens	CAFPs
Walls	0	4
Top/bottom layers	0	5
Infill type	ZigZag	Grid
Infill rate	100%	70%

2.3. Methods and Test Equipment

Flexural and tensile tests were performed on a 100 KN INSTRON machine. This machine is equipped with an AVE 2 Extensometer to measure local strains. Tests were performed according to the following standards: 1 mm/s for the tensile specimens and 2 mm/s for the flexural specimens [21,22]. The raw data of the tests were computed using BlueHill Universal 3 software. For tensile tests, Young's modulus, tensile strength, and elongation at break were studied. For the flexural tests, flexural modulus, flexural strength, conventional deflection, and flexural stress at conventional deflection were reported.

The conventional deflection f is calculated according to the following equation [22]:

$$f = \frac{\varepsilon_f * L^2}{600 * e} \quad (1)$$

where ε_f is the flexural elongation, L is the span, and e is the thickness of the specimen. The set-up of the measures is displayed in Figure 6.

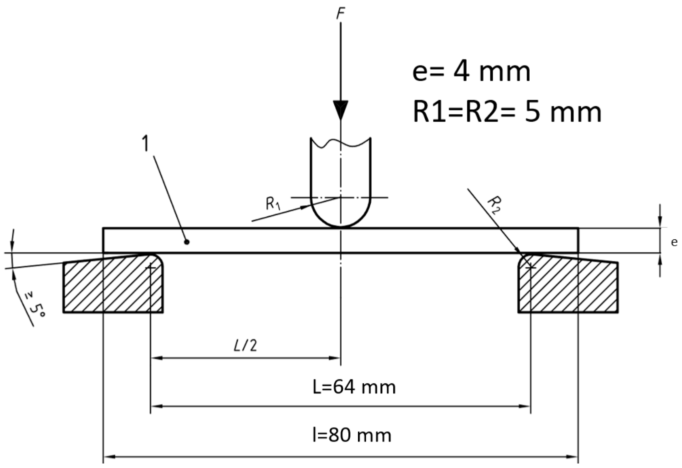

Figure 6. Dimensions of the experiment provided by ISO 178 test standard [22].

The density measurements were performed according to the ISO 1183 test standard. In Figure 7, the scale OHAUS (supplied by OHAUS, Nänikon, Switzerland) was used with its density kit. The specimens are first weighed in air then immerged in water. The measurements were made in a 23 °C environment. The density of the specimen ρ_S is calculated according to the following equation [23]:

$$\rho_S = \frac{m_{S,A} * \rho_{IL}}{m_{S,A} - m_{S,IL}} \quad (2)$$

where $m_{S,A}$ is the apparent mass of the specimen in the air, $m_{S,IL}$ is the apparent mass of the specimen in the liquid, and ρ_{IL} is the water density at 23 °C, which is 0.998 g/cm^3 according to the supplier of the kit.

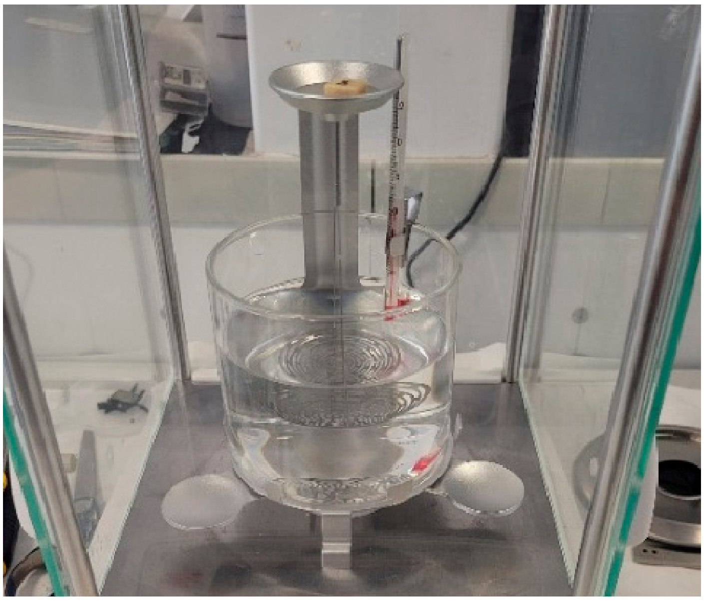

Figure 7. Picture of the scale used for the density measurements.

The DSC is performed on a TA INSTRUMENT Q100 on a 7 mg PEKK-A sample. Analysis was completed under nitrogen from 30 °C to 400 °C at a heating rate of 10 °C/min, kept 3 min, and then cooled from 400 °C to 30 °C at 10 °C/min. The results were analyzed with TA Universal Analysis 2000 software.

Heat flow Δq is obtained through the basis of the following equation [24]:

$$\Delta q = \frac{60}{\beta} \int_{T1}^{T2} \frac{dq}{dt} dT \tag{3}$$

where β is the heating or cooling rate and T is the temperature range.

The finite element analyses are performed on ABAQUS V6-14, and the image correlation software used is GOM CORRELATE 2018.

The metrology and tomography studies are made with TOMO RX SOLUTION (supplied by RX Solution, Chavanod, France) from the Southeast Laboratory of SEMATEC, and the results are analyzed on myVGL 2023 software. The metrology analysis compares the CAD of the studied part (in STL format) with its X-ray scan.

3. Results and Discussion

3.1. Thermal Properties

The DSC is performed on the filament to determine its thermal properties. In Figure 8, the thermogram displays a glass transition (T_g) at 149 °C, which is 10 °C lower than the value given by the supplier. Cold crystallization (T_{cc}) occurs at 263 °C with an enthalpy (ΔH_c) of 4.4 J/g. Melting peak (T_m) appears closely after at 308 °C with an enthalpy ΔH_m of 4.7 J/g. There is no crystallization during controlled cooling at 10 °C/min. This general behavior and the values found are coherent with the literature [25–28].

The crystallinity (χ) is usually calculated according to the following equation [29]:

$$\chi = \frac{\Delta H_m}{\Delta H_m^0} \times 100\% \tag{4}$$

However, it cannot be calculated since the melting enthalpy of 100% crystalline PEKK (ΔH_m^0) is still unknown due to the novelty of the polymer. The cold crystallization and melting enthalpy are similar, which indicates that the specimen has low crystallinity.

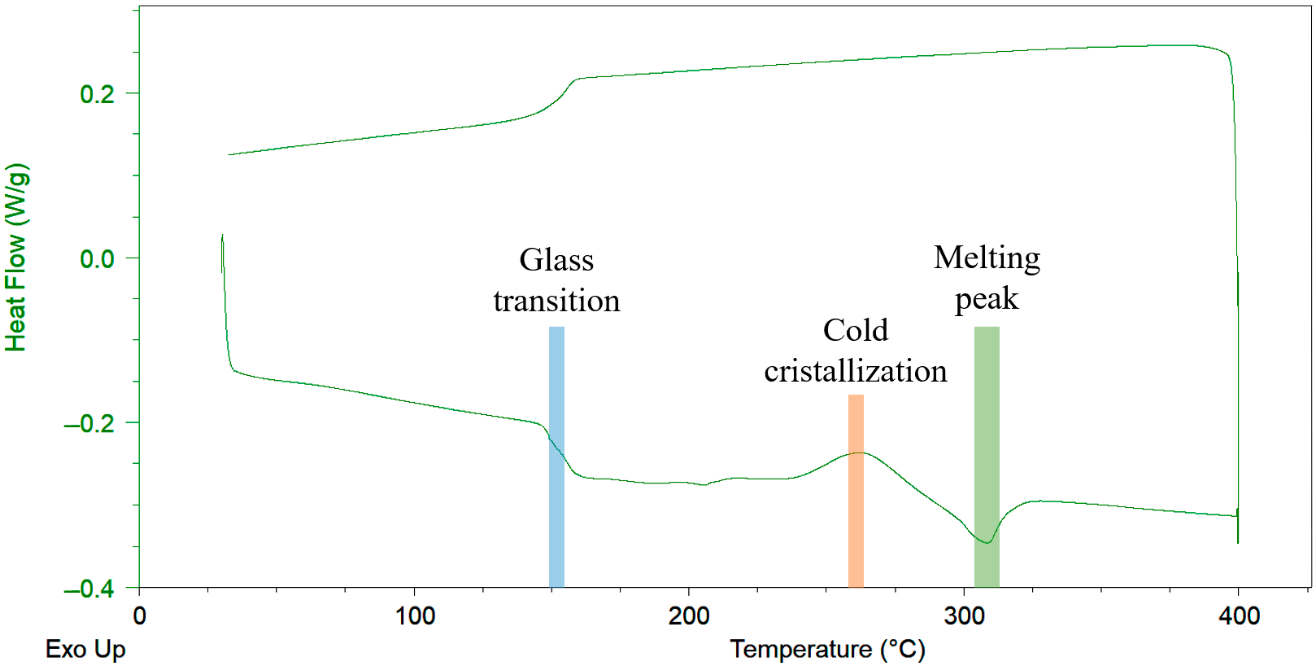

Figure 8. DSC of the PEKK-A filament.

3.2. Mechanical Properties

3.2.1. Flexural Tests

Stress and strain curves are presented in Figure 9. The detailed properties of "flat" (F1–F5) and "on edge" (F6–F10) specimens are displayed in Tables 4 and 5. They show that compared to printing "flat", printing "on edge" improves the flexural modulus by 13%, the flexural strength by 14%, and the stress by 12% at conventional deflection.

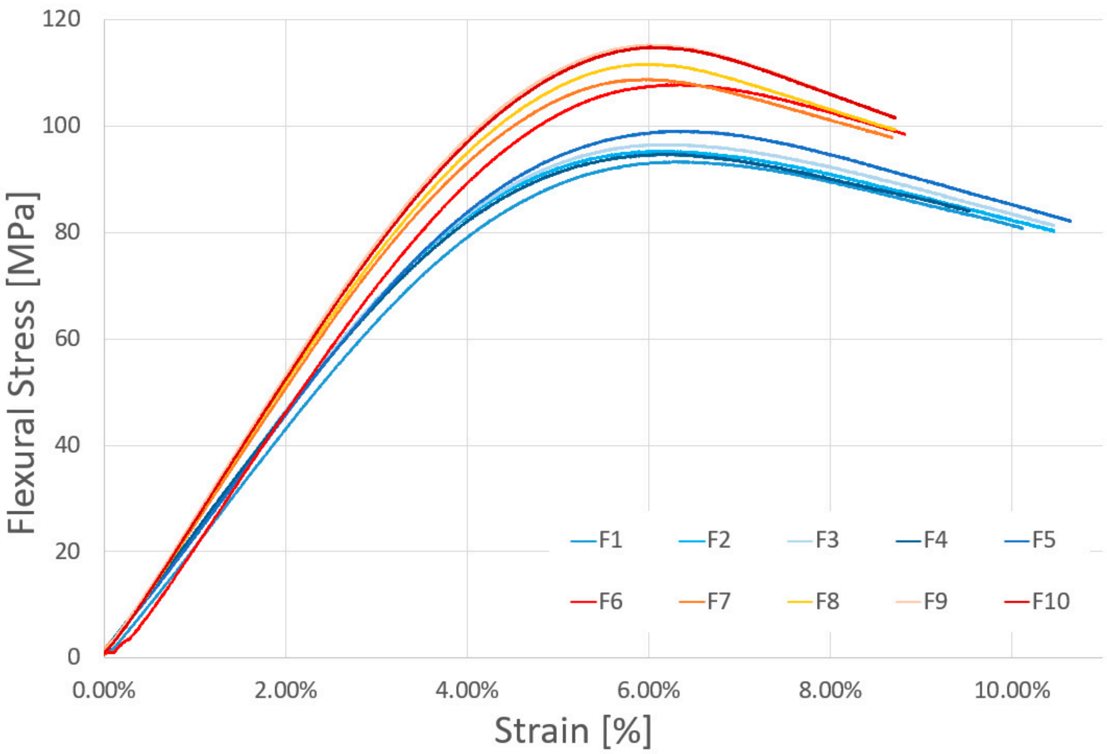

Figure 9. Flexural stress/strain curves of 3D-printed PEKK depending on printing direction.

Table 4. Results of flexural tests for specimen printed "Flat".

Specimen	Flexural Modulus [MPa]	Flexural Strength [MPa]	Conventional Deflection (3.5% Strain) [mm]	Flexural Stress at Conventional Deflection [MPa]
F1	2200	94	5.5	72
F2	2279	95	5.6	76
F3	2289	97	5.6	76
F4	2239	95	5.6	75
F5	2276	99	5.5	76
Mean value	2266	96	5.6	75
Standard deviation	40	2.3	0.04	1.8

Table 5. Results of flexural tests for specimen printed "on edge".

Specimen	Flexural Modulus [MPa]	Flexural Strength [MPa]	Conventional Deflection (3.5% Strain) [mm]	Flexural Stress at Conventional Deflection [MPa]
F6	2526	108	5.2	80
F7	2544	109	5.2	85
F8	2610	112	5.2	86
F9	2670	115	5.4	89
F10	2657	115	5.4	88
Mean value	2601	112	5.2	86
Standard deviation	65	3.4	0.10	3.3

In [30], 3D-printed PEKK is studied but with different printing parameters (±45 raster angle, 90 °C heated chamber, 130 °C bed temperature). The study also concludes that the "on edge" printing direction enhances mechanical properties. With this printing direction, the inter-layer cohesion allows an even distribution of normal and shear stresses between layers that leads to intralayer tensile and shear failures.

Between neat [31] and 3D-printed PEKK, there is a −30% difference for specimens printed "flat" and 20% difference for those printed "on edge" for the flexural modulus and the flexural strength. Poor adhesion between layers can be the reason for such deviations.

3.2.2. Tensile Tests

In Figure 10, the stress and strain curves of specimens T1 to T10 are presented. According to Tables 6 and 7, the difference for the Young's modulus between specimens printed "flat" and "on edge" is lower, but only by 5%. However, printing "on edge" offers +27% improved performances in tensile strength and a +31% increase in elongation at break.

The surfaces of "on edge" layers are smaller. References [32,33] show the temperature gradient along the printed surfaces. This means that, from one layer to another, "flat" surfaces are cooler than "on edge" surfaces because they are larger. They are then reheated by the new layer printed on top. This phenomenon can impact their crystallinity and thus their mechanical performances. Moreover, chamber temperature of the printer is uncontrolled, which can increase the gradient along the surface. Without proper control, the chamber temperature can be influenced by the duration of printing, the nozzle, and the bed temperature. In [34], parts printed with a chamber temperature under the glass transition had lower crystallinity rates and a lower Young's modulus. Lack of controlled ambient temperature inside the printer could also influence the crystallization of PEKK through the thickness of the part.

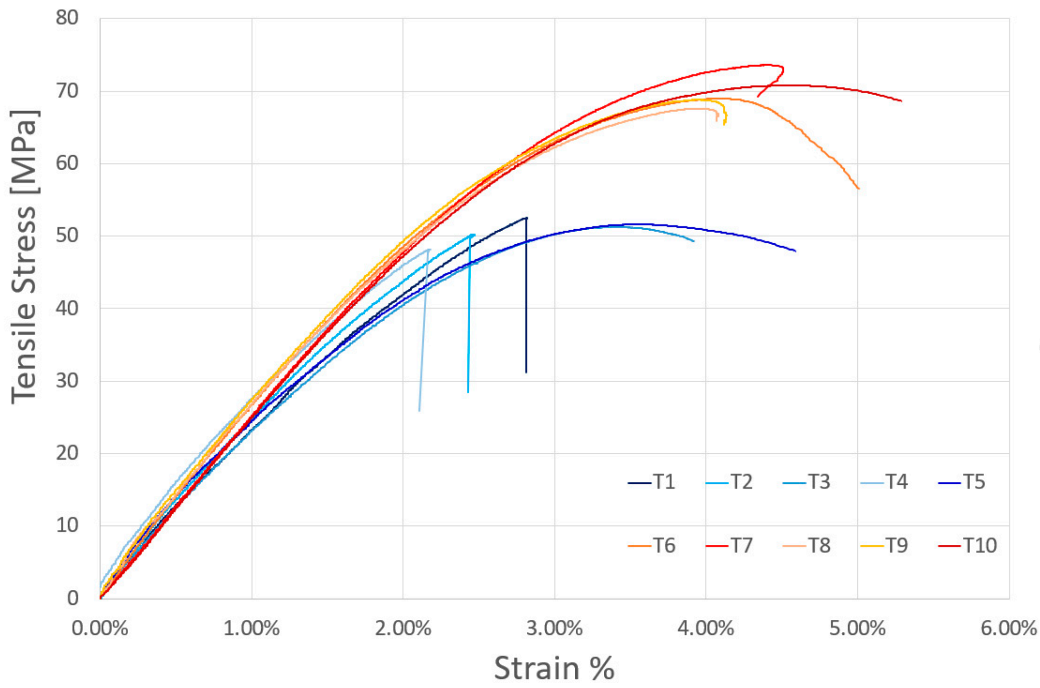

Figure 10. Stress/strain curves of 3D-printed PEKK depending on printing orientation.

Table 6. Results of tensile tests for specimens printed "flat".

Specimen	Young's Modulus [MPa]	Tensile Strength [MPa]	Elongation at Break [%]
T1	2218	53	2.8
T2	2795	50	2.5
T3	2506	51	3.4
T4	2950	48	2.2
T5	2991	52	3.6
Mean value	2692	51	2.9
Standard deviation	326	1.7	0.6

Table 7. Results of tensile tests for specimens printed "on edge".

Specimen	Young's Modulus [MPa]	Tensile Strength [MPa]	Elongation at Break [%]
T6	2892	69	4.1
T7	2474	74	4.4
T8	3420	68	4.0
T9	3027	69	3.9
T10	2351	71	4.5
Mean value	2833	70	4.2
Standard deviation	432	2.3	0.3

This can explain the deviation between injected [35] and 3D-printed PEKK. There is a −33% difference for specimens printed "flat" and a 29% difference for those printed "on edge" for the tensile modulus and the flexural strength. These differences between injected molded and 3D-printed parts have already been observed for other polymers, such as

ABS, PLA, or nylon 6 [36,37]. The porosity induced by the process and the poor adhesion between layers lowers the mechanical properties of these polymers.

3.2.3. Density Measurements

In Figure 11, the density of specimens printed "flat" is 1.07 ± 0.02 g/cm^3 and 1.15 ± 0.01 g/cm^3 for those printed "on edge". This 9% difference could be another explanation for the enhancement of "on edge" mechanical properties. However, it is difficult to know about water absorption due to ambient humidity, even if it is controlled. Thus, more measurements will be made in the future works to validate these results. Moreover, the specimens printed "on edge" are 11% less dense than the PEKK-A filament, confirming the presence of voids caused by the process, as seen in the literature [38]. A tomography analysis is needed to quantify the volume of voids and their distribution.

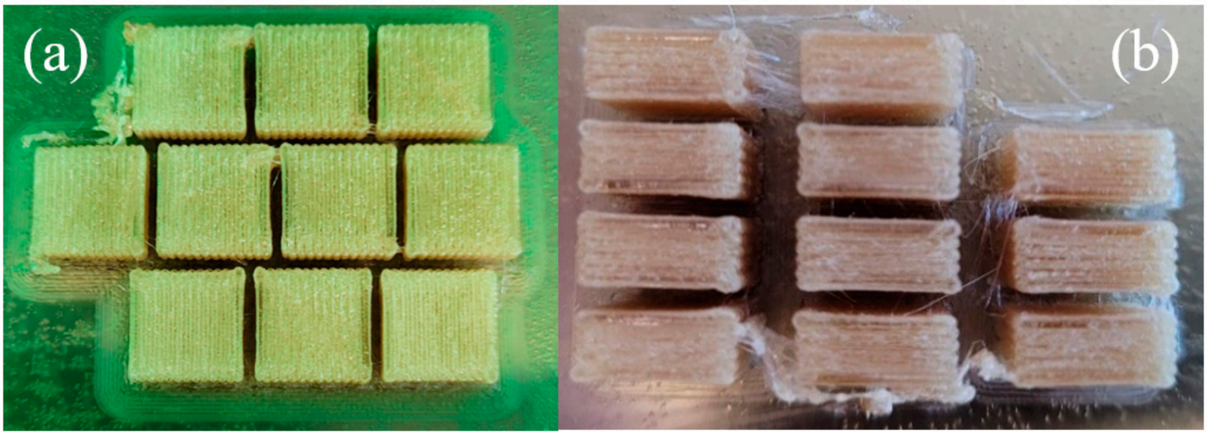

Figure 11. Specimens used for density measurements printed "flat" (**a**) and "on edge" (**b**).

The effects of printing direction on mechanical properties are studied. Printing "on edge" improves both tensile and flexural properties of the specimen as well as its density. These results justify these authors' decision to print the blades of both CAFPs "on edge".

3.3. Finite Element Analysis and Experiment Correlation

In Figure 12, the set-up for the experiments is displayed. For both designs, one extremity of the CAFP is embedded, while a mass of 180g is attached to the other. Pictures of the mechanism deformation are taken, and the experiment is repeated five times. The pictures are analyzed with the image correlation software GOM CORRELATE 2018 where the displacements of the points A, B, and C are measured.

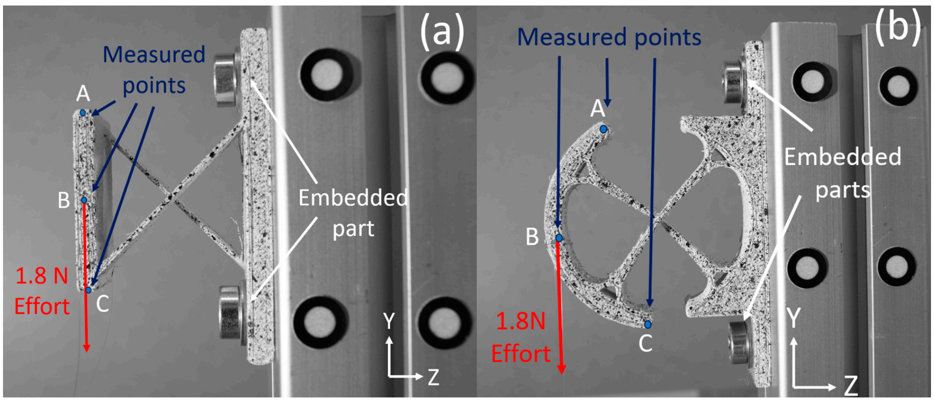

Figure 12. Experimental set-up of CAFP1 (**a**) and CAFP2 (**b**) with the locations of points A, B and C where the displacements are measured.

A static general finite element analysis of the pivots is created using volumic quadratic C3D10 elements. Blades are printed "on edge", so it is assumed that the density and mechanical properties measured in the previous tests are the same. Therefore, the material defined in the model is isotropic, has a Young's modulus of 2833 MPa, and a Poisson's ratio of 0.4 [39]. For CAFP1, free tetrahedral elements of this model have different lengths: 0.5 mm for the blades and 1.5 mm for the rest of the pivot. For CAFP2, the blades have elements around 0.5 mm and 1 mm for the rest of the model. A total of 296,593 nodes and 161,182 elements are used for CAFP1, and 244,432 nodes and 161,053 elements are used for the CAFP2. The boundary conditions are the same as for the experiment presented in Figure 12: an effort of 1.8 N is applied at the drilling site at Point B, and the two other drillings are constrained in every DOF. The distance covered by Points A and C are measured between the neutral fiber and the circular arc of the extremities of the geometries, while Point B is measured at the drilling site.

In Figure 13 and Table 8, the displacements of the CAFP1 model have less than 10% difference with the experiments. If these results are satisfactory, the model still can be perfected by considering the anisotropy of the material [11].

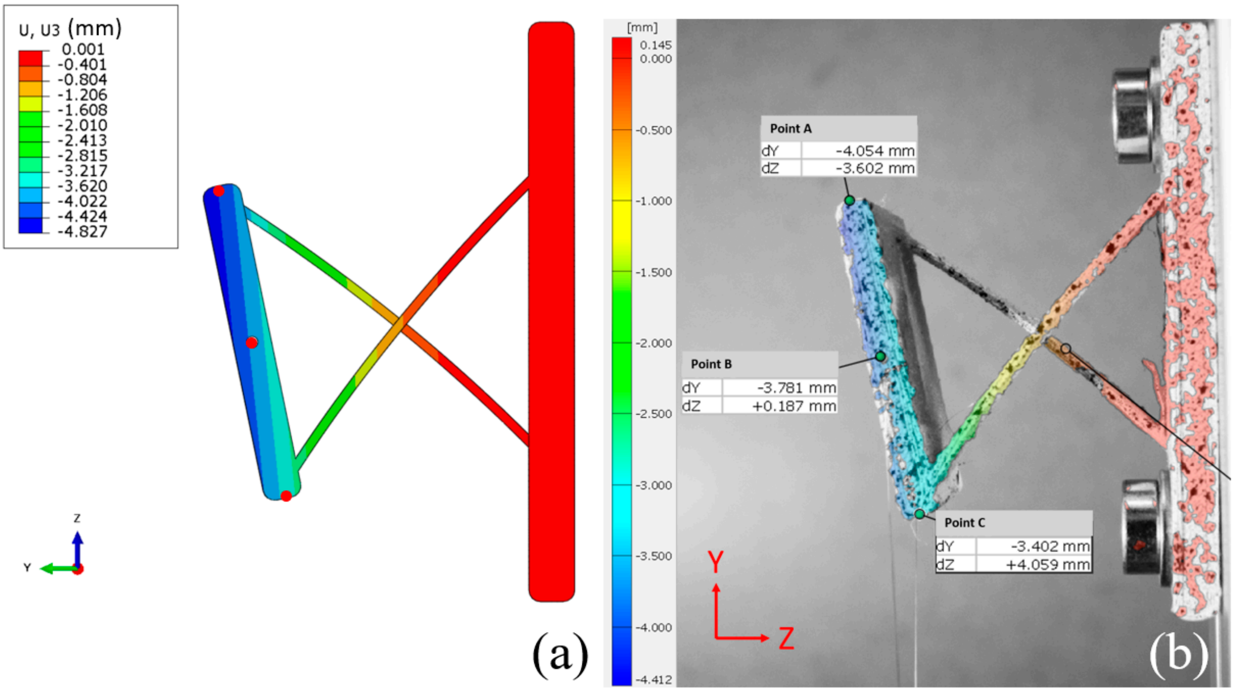

Figure 13. CAFP1: comparison between the finite element analysis model (**a**) and one of the tests analyzed on GOM CORRELATE (**b**).

Table 8. Tests versus model results of CAFP1.

	AY	AZ	BY	BZ	CY	CZ
Displacement test [mm]	−4.21	−3.71	−3.73	0.23	−3.42	3.97
Standard deviation [mm]	0.27	0.27	0.29	0.06	0.19	0.20
Displacement model [mm]	−4.55	−3.99	−3.93	0.19	−3.31	4.36
Difference	−8%	−7%	−5%	17%	3%	−10%

In Figure 14 and Table 9, the difference increases from 3% to 20%, which is higher than the previous model. These deviations can be explained by the complexity of the geometry. During slicing, the software makes an estimation of the geometry with the given parameters, so it is possible that parts of the design are left out. Another cause could be an embrittlement of the blades when the supports are taken out. Metrology and tomography studies are needed to confirm these theories.

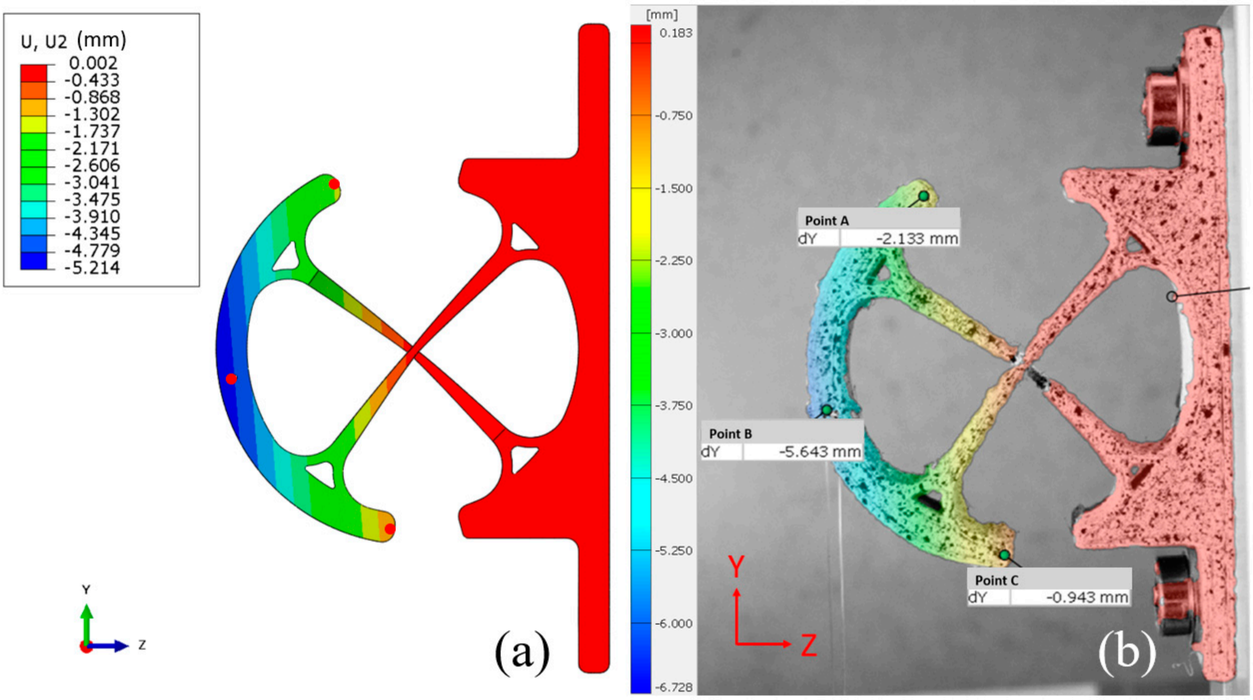

Figure 14. CAFP2: comparison between the finite element analysis model (**a**) and one of the tests analyzed on GOM CORRELATE (**b**).

Table 9. Tests versus model results of CAFP2.

	AY	AZ	BY	BZ	CY	CZ
Mean distance test [mm]	−2.34	−5.14	−5.68	0.76	−1.00	5.43
Standard deviation [mm]	0.09	0.31	0.10	0.29	0.06	0.31
Distance model [mm]	−1.88	−4.54	−4.79	0.413	−1.03	4.596
Difference	20%	12%	16%	46%	−3%	15%

3.4. Metrology Analysis

To investigate tests and model deviation, a comparison between the CAD of both CAFP designs and the scan of their 3D-printed twin is made. In Figure 15, the views of the bottom face are presented for both CAFPs, which is the surface that is facing the bed of the printer and the view of the top face. Pink sections of the analysis are considered "out of range". They are either excess stringing material that was not taken off before the analysis or they are extruded material when drilling the specimen before setting it up for the previous tests.

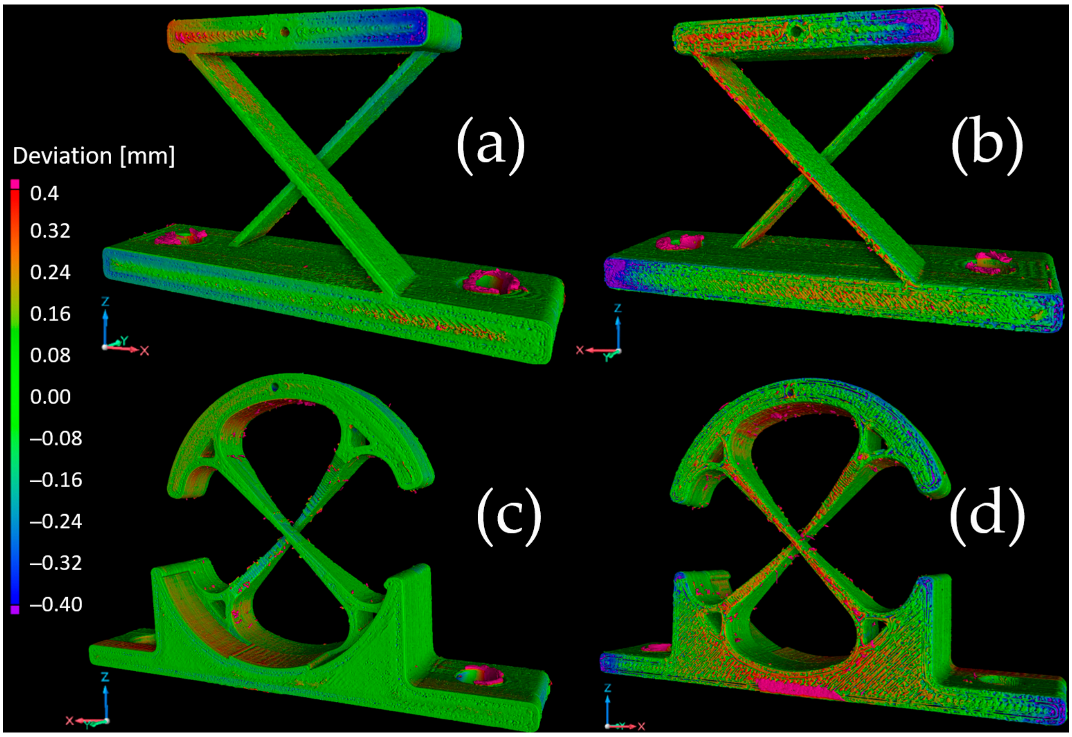

Figure 15. Deviation between CAD and 3D-printed CAFPs: (**a**) top facing view of CAFP1, (**b**) bottom facing view of CAFP1, (**c**) top facing view of CAFP2, (**d**) bottom facing view of CAFP2.

The analysis of these scans is focused on the blades of the CAFPs. Figure 16 displays the surfaces that are studied for CAFP2. They are the same for the standard design. Twenty measures are taken on each surface, and their mean deviations are provided in Figure 17. For both designs, the studied surfaces have a mean deviation in an interval from −0.10 mm to +0.10 mm, which is considered sufficient knowing that the layer's thickness is 0.2 mm. However, their standard deviations are high, which corresponds to the irregularity of the surfaces. Deviations from areas 1 and 3 are the highest. Indeed, these surfaces are in direct contact with the supports, and some of them might have stayed attached to the surfaces during their removal. Their standard deviations are also the highest. The irregularity of their surface can be observed in Figure 15. Area 7 also stands out for CAFP2 as the curves of the blade had to be sliced, which resulted in a lack of material compared to the CAD.

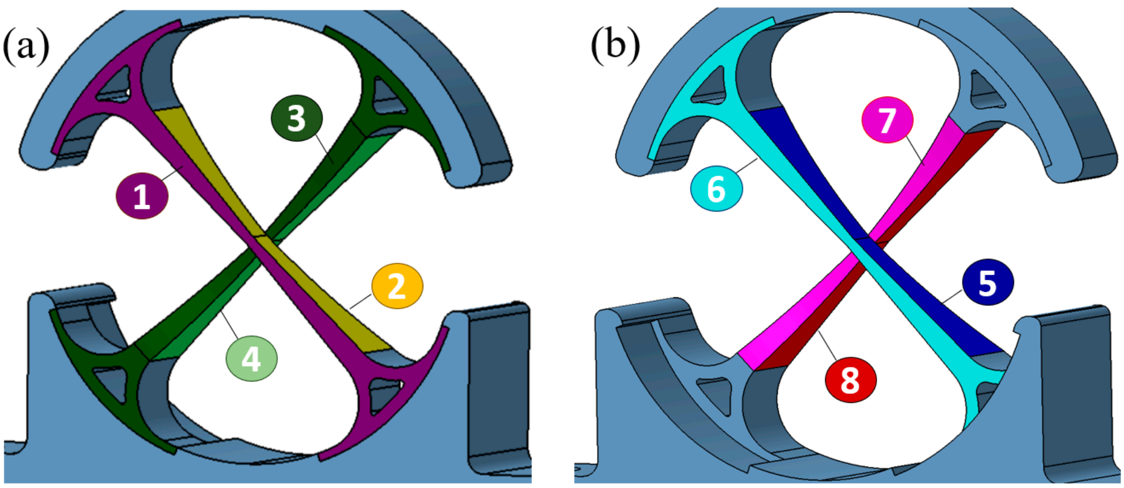

Figure 16. Studied surfaces (1 to 8) for the deviation study: (**a**) view of the surface facing towards the printing bed and (**b**) view of the top surface.

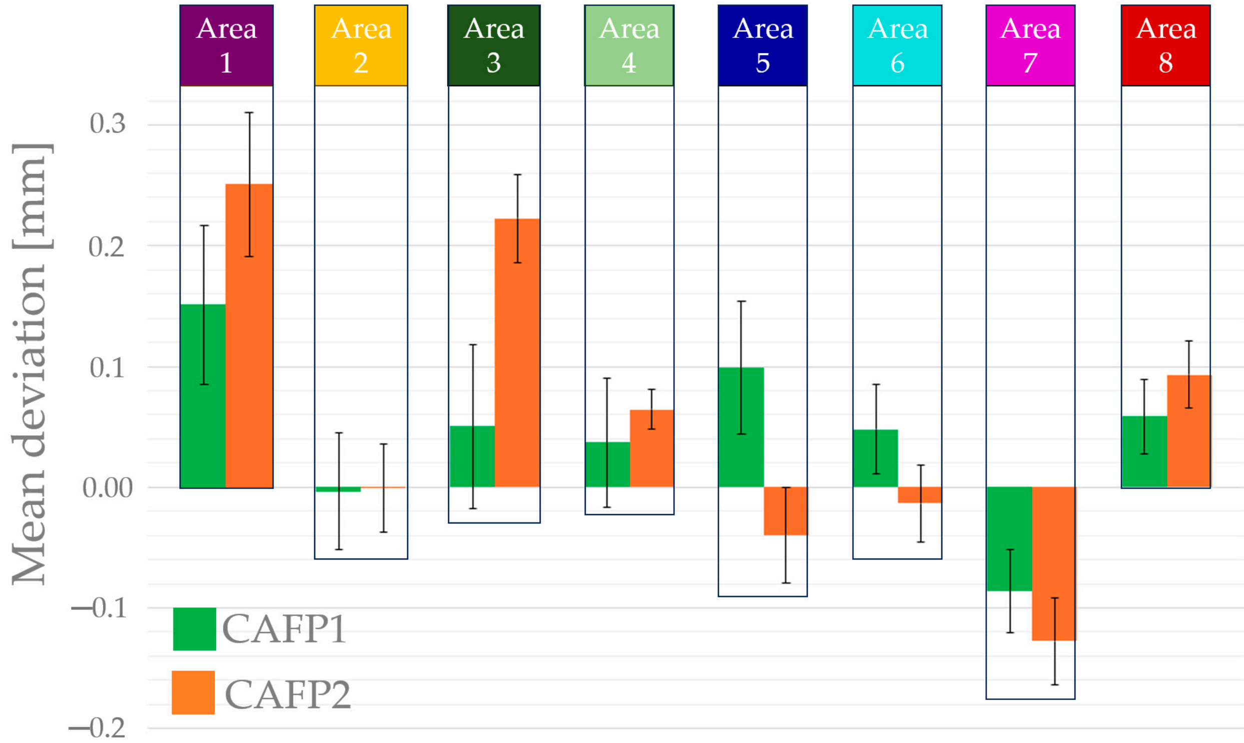

Figure 17. Comparison of the mean deviation in different surfaces for both CAFPs.

The overall deviation is low enough, so the impact on the inertia does not impact the mechanical behavior of the mechanism. Even if the accuracy of the 3D printer needs to be studied further, it does not seem to be the source of the test versus model differences.

A preliminary analysis of X-ray tomography of the two studied designs is carried out. In Figures 18 and 19, slices of the design are shown. In black, voids inside the material are visible. Thus, the grid infill is seen on both sides of the blades. However, by zooming in on the walls and the blades, what seem like voids can be spotted, especially for CAFP2. According to the printing parameters, the blades should be 100% filled. These voids are not considered in the model but could be essential in the mechanical behavior of the CAFPs. Indeed, they could facilitate the propagation of cracks in the blades. Further analyses will be pursued in future works by studying simpler specimens and the impacts of printing parameters on porosity.

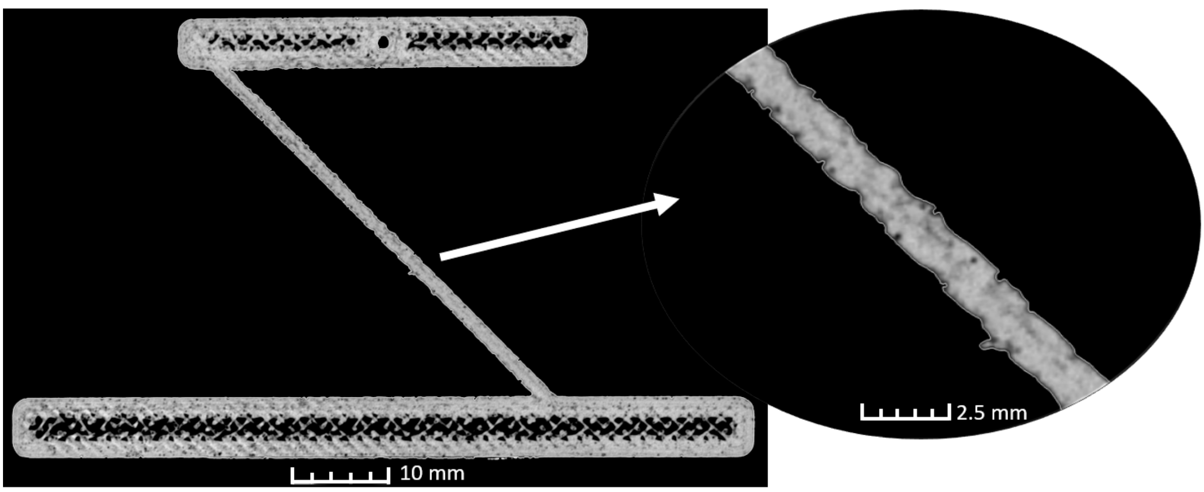

Figure 18. X-ray tomography of CAFP1.

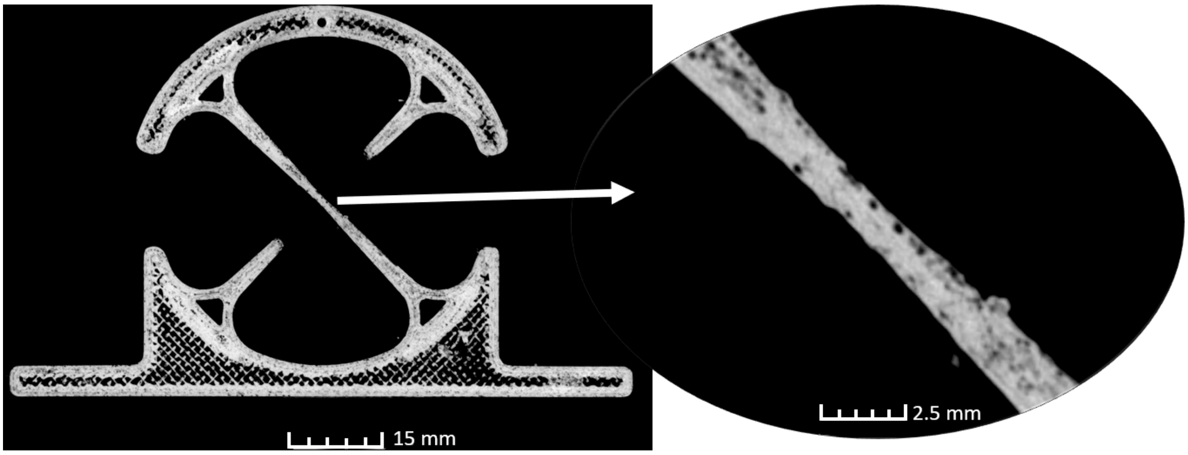

Figure 19. X-ray tomography of CAFP2.

4. Conclusions

The authors' work goes through several steps in the development of a potential spatializable compliant mechanism printed with PEKK. This study focuses on the creation of an accurate finite element model of the CAFP. First, thermal analysis confirmed PEKK's high temperature properties. Then, the influence of printing direction was highlighted through tensile and flexural tests. Printing "on edge" improves the flexural modulus by 13% and tensile strength by 27%.

With the previous data, a finite element model of the CAFP was created and compared to the experiments. It was validated for the standard version of the CAFP (with less than 10% test/model error). Although these results are satisfying, improvements can be made for CAFP2. If the first lead was targeted on geometry accuracy, a scan analysis revealed that the overall deviation between the CAD and the 3D-printed model was below 0.1 mm, which is not enough to influence the model. However, a preliminary tomography study displayed the presence of voids inside the blades of the CAFPs, which could have an impact on mechanical behavior. Other leads on improving our results can consider the anisotropy of the material in the model and the impact of uncontrolled chamber temperature on mechanical properties to investigate a way to balance its effects.

Our future works will focus on deepening these findings by studying the effects of printing parameters on the distribution and quantity of voids through X-ray tomography. Thermal vacuum tests will be performed as vacuum resistance is a key requirement for the spatialization of 3D-printed systems.

Author Contributions: Conceptualization: M.D.; methodology: M.D., A.D.G., and B.O.; validation: Y.-H.G., Y.J., and B.O.; formal analysis: M.D.; investigation: M.D. and B.O.; writing—original draft preparation: M.D.; writing—review and editing: Y.-H.G., Y.J., and B.O.; supervision, Y.J. and B.O. All authors have read and agreed to the published version of the manuscript.

Funding: This research received no external funding.

Data Availability Statement: The raw data supporting the conclusions of this article will be made available by the authors on request.

Acknowledgments: The authors gratefully thank the Région Sud–Provence Alpes Côte d'Azur for its financial support through the co-financing of Morgane Domerg's thesis, which was supported by the company CES WORKS and was carried out within the MAPIEM laboratory of the University of Toulon, France. The authors also thank the team of the South-East lab of SEMANTEC that is part of Hexagon for their contribution with the tomography analyses.

Conflicts of Interest: Author Antoine Dubois Garcia was employed by the company Hexagon. Author Yves-Henri Grunevald was employed by the company CES WORKS. The remaining authors declare that this research was conducted in the absence of any commercial or financial relationships that could be construed as potential conflicts of Interest.

Abbreviations

DOF	Degree of freedom
CAFP	Cross-axis flexural pivot
PEKK	Polyetherketoneketone
PEEK	Polyetheretherketone
PLA	Poly(lactic acid)
FFF	Fused filament fabrication
TGA	Thermogravimetric analysis
DSC	Differential scanning calorimetry
FTIR	Fourier transform infrared
CAD	Computer-Aided Design

List of Symbols

χ	Degree of crystallinity [%]
ΔH_m	Experimental melting enthalpy [J/g]
ΔH_m^0	Melting enthalpy of a 100% crystalline material [J/g]
ΔH_c	Enthalpy of crystallization [J/g]
Tg	Glass transition temperature [°C]
Tc	Crystallization temperature [°C]
Tm	Melting temperature [°C]

References

1. Dearden, J.; Grames, C.; Jensen, B.D.; Magleby, S.P.; Howell, L.L. Inverted L-Arm Gripper Compliant Mechanism. *J. Med. Devices* **2017**, *11*, 034502. [CrossRef]
2. Merriam, E.G.; Jones, J.E.; Magleby, S.P.; Howell, L.L. Monolithic 2 DOF Fully Compliant Space Pointing Mechanism. *Mech. Sci.* **2013**, *4*, 381–390. [CrossRef]
3. Dang, M.P.; Le, H.G.; Van, M.N.; Chau, N.L.; Dao, T.-P. Modeling and Optimization for a New Compliant 2-Dof Stage for Locating Biomaterial Samples by an Efficient Approach of a Kinetostatic Analysis-Based Method and Neural Network Algorithm. *Comput. Intell. Neurosci.* **2022**, *2022*, 6709464. [CrossRef] [PubMed]
4. Hao, G.; Yu, J.; Li, H. A Brief Review on Nonlinear Modeling Methods and Applications of Compliant Mechanisms. *Front. Mech. Eng.* **2016**, *11*, 119–128. [CrossRef]
5. Jensen, B.D.; Howell, L.L. The Modeling of Cross-Axis Flexural Pivots. *Mech. Mach. Theory* **2002**, *37*, 461–476. [CrossRef]
6. Dearden, J.; Grames, C.; Orr, J.; Jensen, B.D.; Magleby, S.P.; Howell, L.L. Cylindrical Cross-Axis Flexural Pivots. *Precis. Eng.* **2018**, *51*, 604–613. [CrossRef]
7. Wu, J.; Cai, S.; Cui, J.; Tan, J. A Generalized Analytical Compliance Model for Cartwheel Flexure Hinges. *Rev. Sci. Instrum.* **2015**, *86*, 105003. [CrossRef] [PubMed]
8. Corapi, D.; Morettini, G.; Pascoletti, G.; Zitelli, C. Characterization of a Polylactic Acid (PLA) Produced by Fused Deposition Modeling (FDM) Technology. *Procedia Struct. Integr.* **2019**, *24*, 289–295. [CrossRef]
9. Wang, P.; Zou, B.; Ding, S.; Li, L.; Huang, C. Effects of FDM-3D Printing Parameters on Mechanical Properties and Microstructure of CF/PEEK and GF/PEEK. *Chin. J. Aeronaut.* **2021**, *34*, 236–246. [CrossRef]
10. Hanon, M.M.; Dobos, J.; Zsidai, L. The Influence of 3D Printing Process Parameters on the Mechanical Performance of PLA Polymer and Its Correlation with Hardness. *Procedia Manuf.* **2021**, *54*, 244–249. [CrossRef]
11. Forés-Garriga, A.; Pérez, M.A.; Gómez-Gras, G.; Reyes-Pozo, G. Role of Infill Parameters on the Mechanical Performance and Weight Reduction of PEI Ultem Processed by FFF. *Mater. Des.* **2020**, *193*, 108810. [CrossRef]
12. Abeykoon, C.; Sri-Amphorn, P.; Fernando, A. Optimization of Fused Deposition Modeling Parameters for Improved PLA and ABS 3D Printed Structures. *Int. J. Lightweight Mater. Manuf.* **2020**, *3*, 284–297. [CrossRef]
13. Zhen, H.; Zhao, B.; Quan, L.; Fu, J. Effect of 3D Printing Process Parameters and Heat Treatment Conditions on the Mechanical Properties and Microstructure of PEEK Parts. *Polymers* **2023**, *15*, 2209. [CrossRef] [PubMed]
14. Battes, K.; Day, C.; Hauer, V. Outgassing Behavior of Different High-Temperature Resistant Polymers. *J. Vac. Sci. Technol. A Vac. Surf. Film.* **2018**, *36*, 021602. [CrossRef]
15. Lafont, U.; Munck, M.; Wessing, J.; Terol-Sanchez, M.; Rampini, R. 3D Printing of Multifunctional Polymer for Space Application. In Proceedings of the 9th European Conference for Aeronautics and Space Sciences (EUCASS), Lille, France, 27 June–1 July 2022; p. 13. [CrossRef]
16. Rinaldi, M.; Cecchini, F.; Pigliaru, L.; Ghidini, T.; Lumaca, F.; Nanni, F. Additive Manufacturing of Polyether Ether Ketone (PEEK) for Space Applications: A Nanosat Polymeric Structure. *Polymers* **2020**, *13*, 11. [CrossRef] [PubMed]
17. Pérez-Martín, H.; Mackenzie, P.; Baidak, A.; Ó Brádaigh, C.M.; Ray, D. Crystallinity Studies of PEKK and Carbon Fibre/PEKK Composites: A Review. *Compos. Part B Eng.* **2021**, *223*, 109127. [CrossRef]

18. Pedoto, G. *Characterization and Modelling of the Thermomechanical and Ageing Behavior of PEKK and C/PEKK Composites for Aircraft Applications at High Temperatures (Above the Glass Transition Temperature)*; ISAE-ENSMA Ecole Nationale Supérieure de Mécanique et d'Aérotechique: Poitiers, France, 2020.
19. Alqurashi, H.; Khurshid, Z.; Syed, A.U.Y.; Rashid Habib, S.; Rokaya, D.; Zafar, M.S. Polyetherketoneketone (PEKK): An Emerging Biomaterial for Oral Implants and Dental Prostheses. *J. Adv. Res.* **2021**, *28*, 87–95. [CrossRef] [PubMed]
20. Cheng, K.; Shi, Z.; Wang, R.; Jiang, X.; Xiao, F.; Liu, Y. 3D Printed PEKK Bone Analogs with Internal Porosity and Surface Modification for Mandibular Reconstruction: An in Vivo Rabbit Model Study. *Biomater. Adv.* **2023**, *151*, 213455. [CrossRef] [PubMed]
21. *International Organization for Standardization ISO 527-1:2012*; Plasics—Determination of Tensile Properties—Part 2: Test Conditions for Moulding and Extrusion Plastics. ISO: Geneva, Switzerland, 2012.
22. *International Organisation for Standardization ISO 178*; Plastics—Determination of Flexural Properties. ISO: Geneva, Switzerland, 2006.
23. *International Organisation for Standardization ISO 1183-1*; Plastics—Methods for Determining the Density of Non-Cellular Plastics—Part 1: Immersion Method, Liquid Pycnometer Method and Titration Method. ISO: Geneva, Switzerland, 2019.
24. *International Organisation for Standardization ISO 11357-1:2016(En)*; Plastics—Differential Scanning Calorimetry (DSC)—Part 1: General Principles. ISO: Geneva, Switzerland, 2016.
25. Yahiaoui, M.; Chabert, F.; Paris, J.-Y.; Nassiet, V.; Denape, J. Friction, Acoustic Emission, and Wear Mechanisms of a PEKK Polymer. *Tribol. Int.* **2019**, *132*, 154–164. [CrossRef]
26. Vasconcelos, G.d.C.; Mazur, R.L.; Botelho, E.C.; Rezende, M.C.; Costa, M.L. Evaluation of Crystallization Kinetics of Polymer of Poly (Ether-Ketone-Ketone) and Poly (Ether-Ether-Ketone) by DSC. *JATM* **2010**, *2*, 155–162. [CrossRef]
27. Alexandre, M. *Optimisation du Comportement Mécanique de Composites Structuraux PEKK/Fibres de Carbone par Ensimage Oligomères de PEKK*; Université Toulouse 3 Paul Sabatier: Toulouse, France, 2017.
28. Corbalan, N. *Mechanical Performances of PEKK Thermoplastic Composites Linked to Their Processing Parameters*; École Nationale Supérieure d'Arts et Métiers: Paris, France, 2017.
29. Mngomezulu, M.E.; Luyt, A.S.; John, M.J. Morphology, Thermal and Dynamic Mechanical Properties of Poly(Lactic Acid)/Expandable Graphite (PLA/EG) Flame Retardant Composites. *J. Thermoplast. Compos. Mater.* **2019**, *32*, 89–107. [CrossRef]
30. Xu, C.; Cheng, K.; Liu, Y.; Wang, R.; Xu, X. Effect of Processing Parameters on Flexural Properties of 3D-Printed Polyetherketoneketone Using Fused Deposition Modeling. *Polym. Eng. Sci.* **2021**, *61*, 465–476. [CrossRef]
31. Nassir, N.A.; Birch, R.S.; Cantwell, W.J.; Wang, Q.Y.; Liu, L.Q.; Guan, Z.W. The Perforation Resistance of Glass Fibre Reinforced PEKK Composites. *Polym. Test.* **2018**, *72*, 423–431. [CrossRef]
32. Lee, A.; Wynn, M.; Quigley, L.; Salviato, M.; Zobeiry, N. Effect of Temperature History during Additive Manufacturing on Crystalline Morphology of PEEK. *Adv. Ind. Manuf. Eng.* **2022**, *4*, 100085. [CrossRef]
33. Antony Samy, A.; Golbang, A.; Harkin-Jones, E.; Archer, E.; McIlhagger, A. Prediction of Part Distortion in Fused Deposition Modelling (FDM) of Semi-Crystalline Polymers via COMSOL: Effect of Printing Conditions. *CIRP J. Manuf. Sci. Technol.* **2021**, *33*, 443–453. [CrossRef]
34. Choupin, T.; Debertrand, L.; Fayolle, B.; Régnier, G.; Paris, C.; Cinquin, J.; Brulé, B. Influence of Thermal History on the Mechanical Properties of Poly(Ether Ketone Ketone) Copolymers. *Polym. Cryst.* **2019**, *2*, e10086. [CrossRef]
35. Gan, D.; Lu, S.; Song, C.; Wang, Z. Morphologies, Mechanical Properties and Wear of Poly(Ether Ketone Ketone) (PEKK) and Its Composites Reinforced with Mica. *Macromol. Mater. Eng.* **2001**, *286*, 296–301. [CrossRef]
36. Podsiadły, B.; Skalski, A.; Rozpiórski, W.; Słoma, M. Are We Able to Print Components as Strong as Injection Molded?—Comparing the Properties of 3D Printed and Injection Molded Components Made from ABS Thermoplastic. *Appl. Sci.* **2021**, *11*, 6946. [CrossRef]
37. Lay, M.; Thajudin, N.L.N.; Hamid, Z.A.A.; Rusli, A.; Abdullah, M.K.; Shuib, R.K. Comparison of Physical and Mechanical Properties of PLA, ABS and Nylon 6 Fabricated Using Fused Deposition Modeling and Injection Molding. *Compos. Part B Eng.* **2019**, *176*, 107341. [CrossRef]
38. Ding, S.; Zou, B.; Wang, P.; Ding, H. Effects of Nozzle Temperature and Building Orientation on Mechanical Properties and Microstructure of PEEK and PEI Printed by 3D-FDM. *Polym. Test.* **2019**, *78*, 105948. [CrossRef]
39. Villefort, R.F.; Diamantino, P.J.S.; von Zeidler, S.L.V.; Borges, A.L.S.; Silva-Concílio, L.R.; Saavedra, G.; de Siqueira, F.A.; Tribst, J.P.M. Mechanical Response of PEKK and PEEK As Frameworks for Implant-Supported Full-Arch Fixed Dental Prosthesis: 3D Finite Element Analysis. *Eur. J. Dent.* **2021**, *16*, 115–121. [CrossRef]